Desalination and Water Treatment
www.deswater.com

doi: 10.5004/dwt.2018.22367

133 (2018) 80–91
November

Batch desalination of Gulf of Oman diluted salt water using newly prepared graphene oxide–copper oxide nanocomposite

Maryam Khabbazi, Parvin Alizadeh Eslami*

Department of Chemistry, Faculty of Science, Tabriz Branch, Islamic Azad University, Tabriz, Iran, emails: khabbazi3621@gmail.com (M. Khabbazi), sp.alizadeh@iaut.ac.ir (P.A. Eslami)

Received 22 August 2017; Accepted 13 April 2018

ABSTRACT

In this study, graphene oxide–copper oxide (GO–CuO) based efficient nanocomposite was synthesized for the enhanced desalination of Gulf of Oman saline water. The adsorbent was characterized by Raman spectroscopy, X-ray diffraction, field emission scanning electron microscopy, energy-dispersive X-ray spectroscopy, transmission electron microscopy (TEM) and Brunauer–Emmett–Teller–Barrett–Joyner–Halenda (BET–BJH) techniques. The specific surface area was found to be 76.95 m^2/g for newly fabricated nanocomposite using BET technique. Desalination of seawater was carried out under batch adsorption of Na^+ and K^+ using GO–CuO nanocomposite. Additionally, effective parameters on desalination process such as contact time, initial concentration, temperature and pH were comprehensively analyzed. The removal efficiency values for Na^+ and K^+ using 0.1 g of GO–CuO as an adsorbent were obtained as 96.74% and 82.47%, respectively, within 30 min at pH = 7.2. Moreover, the adsorption equilibrium and contact time data were fitted well to the Langmuir isotherm and pseudo-second-order kinetic model, respectively. The analysis from these models suggested monolayer adsorption pattern following a physisorption mechanism for Na^+ and K^+ ions uptake using GO–CuO nanocomposite.

Keywords: Graphene oxide; CuO nanoparticles; Seawater desalination; Adsorption isotherm; Kinetic study

1. Introduction

Recently, shortage of freshwater due to climate changes, industrial activities, food safeties and growth of population has become a main global challenge [1–3]. Although 75% of the earth surface is covered by water, only 3% of it is potable water which can be used for household activities [4]. According to the Food and Agriculture Organization (FAO) report, the number of people suffering from freshwater scarcity until 2025 would reach 1.9 billion. This, probably would lead to serious water originated conflicts. Hence, desalination of seawater would be an effective way to produce freshwater to address the issue of water scarcity [5]. Desalination methods are the cost-effective technologies that can remove or separate the dissolved salts and inorganic species from water sources. There are various methods for seawater desalination including thermal evaporation, distillation, membrane filtration, reverse osmosis, electrodialysis, gas hydrate and solar desalination [3,6,7]. Applying the nanoparticles in the membranes caused to using nanotechnology as an affordable technique for water desalination by researchers [8–10]. Additionally, nanomaterials are frequently used as adsorbents for seawater desalination. Recyclable and inexpensive adsorbents with potential benefits can be used for recovery of valuable elements such as uranium, lithium and boron [11–14]. Nanoadsorbents based on magnetic nanoparticles [15], conductive polymers [16,17], carbon nanotube [18] and graphene were successfully developed for water desalination.

In particular, water permeable graphene oxide membrane is widely applied in salt water treatment with high desalination efficiency [5,19–21]. Graphene oxide provides interesting features including high specific surface area, porous structure, high flexibility and favourable mechanical/chemical stability [5]. Graphene oxide is a single sheet,

* Corresponding author.

sp^2-bonded carbon, two-dimensional nanostructure, with rich delocalize π–π electron stacking and various oxygenated functional groups (carboxyl, hydroxyl, phenyl and epoxy groups) [21,22]. Due to its high specific surface area and functional groups, graphene oxide can adsorb metal ions due to its remarkable adsorption capacity [23,24]. The graphene-based material is successfully applied for salt water desalination by various researchers [25,26].

In order to increase water permeability, antibacterial effects and easy collection of graphene oxide from the high volume of aqueous samples, CuO nanoparticles were dispersed on the graphene oxide sheets. Low-cost CuO nanoparticles possess potential features including water dispersity, easy synthesis, high affinity towards graphene oxide, besides being greener in synthesis approach and an effective antibacterial agent [27,28]. Due to the presence of various types of microorganisms in seawater the stabilizing of antibacterial adsorbents, that is, CuO is essential for desalination. The antibacterial activity of CuO nanoparticles has been demonstrated previously by different research groups [29–31].

In the current study, a simple, fast and low-temperature method was used for the one-pot synthesis of graphene oxide doped CuO nanoparticles (GO–CuO). GO with large π-staking and high specific surface area avoids the aggregation of CuO nanoparticles. Besides, oxygenated functional groups increase the sorption affinity of GO towards cations (i.e., Na^+ and K^+ ions). Additionally, CuO nanoparticles refrain the agglomeration of GO sheets. The Gulf of Oman's salt water desalination experimental process was evaluated under adsorption isotherms and kinetic models. This study is focused on Na^+ and K^+ ions adsorption from seawater because of high level of sodium and potassium ions.

2. Experimental

2.1. Material and reagents

Ethanol, sodium carbonate (Na_2CO_3), copper(II) nitrate pentahydrate ($Cu(NO_3)_2.5H_2O$), sulphuric acid (H_2SO_4), sodium nitrate ($NaNO_3$), potassium permanganate ($KMnO_4$), hydrogen peroxide (H_2O_2), hydrochloric acid (HCl), dimethylformamide (DMF), chloroform (CH_3Cl) and sodium chloride (NaCl) were purchased from Merck (Darmstadt, Germany). Commercial graphite powder was obtained from Beijing Chemical Co. (Beijing, China).

The Gulf of Oman water samples were collected from the beach of Chabahar, Iran; the native concentration of selected ions was estimated to be 18,700 mg/L for Na^+ and 9,200 mg/L for K^+ ions, pH = 7.2. Working solution was prepared by dilution of seawater (10 times) to get Na^+ = 1,870 mg/L and K^+ = 920 mg/L.

2.2. Characterization of the adsorbent

An atomic emission spectrometer of PFP7 JENWAY with a flame photometer (Leverkusen, Germany) was used for potassium (K) and sodium (Na) level measurements in water samples. The Raman spectra were recorded by an Almega Thermo Nicolet Dispersive spectrometer (Germany). The crystallinity of the nanocomposite was studied using a X'Pert Pro, X-ray diffractometer (XRD) from PANalytical (Almelo, Netherland) with Cu Kα radiation (λ = 1.54060 Å), 40 kV and 40 mA. The specific surface area of the graphene-based adsorbent was studied based on Brunauer–Emmett–Teller (BET) theory by a Microtrac Bel Corp from BElSORP Mini (Tokyo, Japan). A field emission scanning electron microscopy (FESEM) equipped with energy-dispersive X-ray (EDX) analysis from Zeiss SIGMA VP (Jena, Germany) was used for the adsorbent's surface morphology study and element analysis. Nanocomposite morphology was analyzed by a transmission electron microscopy (TEM) from Zeiss-EM10C-100 KV (Oberkochen, Germany) with an accelerating voltage of 80 kV.

2.3. Synthesis of nanocomposite

2.3.1. Synthesis of graphene oxide

Graphite powder (2 g) was dispersed in 50 mL of H_2SO_4 (97%) then 2 g sodium nitrate was added to the mixture. After 1 h of stirring, the mixture was kept in an ice bath and $KMnO_4$ (3.7 g) was slowly added to it. Then, the solution was kept at 35°C for 2 h under vigorous stirring. 140 mL deionized water was added to the mixture before cooling down to the room temperature. Lastly, 6 mL H_2O_2 (30%) was added to the mixture under stirring for 2 h. Then, the product was sonicated for 30 min, thereafter, it was washed with HCl (1%) and deionized water to reach pH ~7. The solid product was oven dried at 40°C for 24 h.

2.3.2. Synthesis of CuO nanoparticles

A copper nitrate solution of 1 M was prepared and slowly added into sodium carbonate solution (1 M) in a preheated water bath at 70°C. The addition rate was approximately 5 mL/min and pH was maintained at 7–8. The sediment was washed and then oven dried at 80°C for 24 h. Thereafter, the product was calcinated at 350°C for 6 h to produce CuO nanoparticles. Finally, the product was grinded into powder and washed with ethanol/water and dried at 60°C for 24 h in a vacuum oven.

2.3.3. Synthesis of CuO doped graphene oxide

50 mg of freshly prepared graphene oxide (GO) was dispersed in 4 mL dimethylformamide and sonicated at room temperature for 2 h. In another vial, 40 mg of CuO nanoparticles was dispersed in 6 mL chloroform then added into GO solution (dropwise) followed by sonication at room temperature for 3 h. Finally, the sediment (GO–CuO) was separated by the assistance of centrifugation and washed with hexane for three times.

2.4. Desalination procedure

The desalination of seawater (50 mL) from Na^+ and K^+ ions was carried out using batch adsorption technique employing 0.1 g GO–CuO nanocomposite at room temperature for 60 min (ultrasonic). The desalination efficiency was investigated by altering various parameters such as pH (5–8), adsorption time (5–60 min) and temperature (25°C–50°C). Hence, after each desalination, the residual concentrations of Na^+ and K^+ ions were measured using flame atomic emission spectroscopy. Finally, the equilibrium adsorption capacity

(q_e) of GO–CuO and adsorption (desalination) efficiency (E%) was calculated using Eqs. (1) and (2), respectively.

$$q_e = \frac{V}{m}(C_0 - C_e) \tag{1}$$

$$E\% = \left(\frac{C_0 - C_e}{C_0}\right) \times 100 \tag{2}$$

where q_e is adsorption capacity (mg/g), V is the aqueous volume (L), m is the mass of adsorbent (g), C_0 initial concentration of ions (mg/L) and C_e concentration of ions after desalination (mg/L).

3. Results and discussions

3.1. Raman spectroscopy

The Raman spectrum of the graphene oxide nanosheets (Fig. 1(A)) shows two peaks for D and G bands at 1,320 and 1,770 cm^{-1}, respectively. The D band is due to the presence of turmoil and flaws in the structure of the graphene network. This mode (D) corresponds to the carbon atoms bonded to oxygen functional groups. The G band is related to the carbon atoms with sp^2 hybridization, in other words, this mode confirms the existence of unreacted carbon atoms on the graphene network. A broad peak at 2,737 cm^{-1} is corresponding to D overtones. Fig. 1(B) shows the Raman spectrum of graphene oxide doped with copper oxide nanoparticles (GO–CuO). It is clear that the two extra characteristic peaks at 596 and 597 cm^{-1} are observed which are corresponding to vibrational modes T_{2g} of copper oxide nanoparticles. The D and G bands are also observed in Fig. 1(B) which confirms the successful synthesis of GO–CuO nanocomposite.

3.2. X-ray diffraction

X-ray diffraction (XRD) is a crucial technique to identify the crystalline structure of nanomaterials. The XRD patterns of the as-prepared CuO nanoparticles (JCPDS Card No. 00-041-0254) and GO–CuO nanocomposite are shown in Figs. 1(C) and (D), respectively. Several sharp peaks are clearly observed for CuO at 2θ = 32.51 (110), 33.55 (002), 38.77 (111), 48.87 (200), 53.44 (111), 58.30 (202), 61.59 (020), 65.68 (113), 66.32 (311), 68.02 (222), 72.41 (311) and 75.73 (222). Only one extra peak at 8.44 (002) was observed in the XRD spectrum of GO–CuO nanocomposite confirming the presence of amorphous graphene oxide. Adsorbent material after desalination was also checked by XRD technique (Fig. 1(E)), it is obvious that two new signals were appeared. These signals are probably due to the adsorption of Na^+ and K^+ on the surface of GO–CuO nanocomposite.

Scherrer's equation (Eq. (3)) was used to predict the average size of CuO crystals as follows:

$$D = \frac{K\lambda}{\beta\cos(\theta)} \tag{3}$$

$$\beta = \text{FWHM} * \left(\frac{\pi}{180}\right) \tag{4}$$

where D is the particle size in nm, θ is the angle corresponding to sharp peaks, λ is the wavelength in nm, FWHM is full-width data at half maximum and K is a constant with the

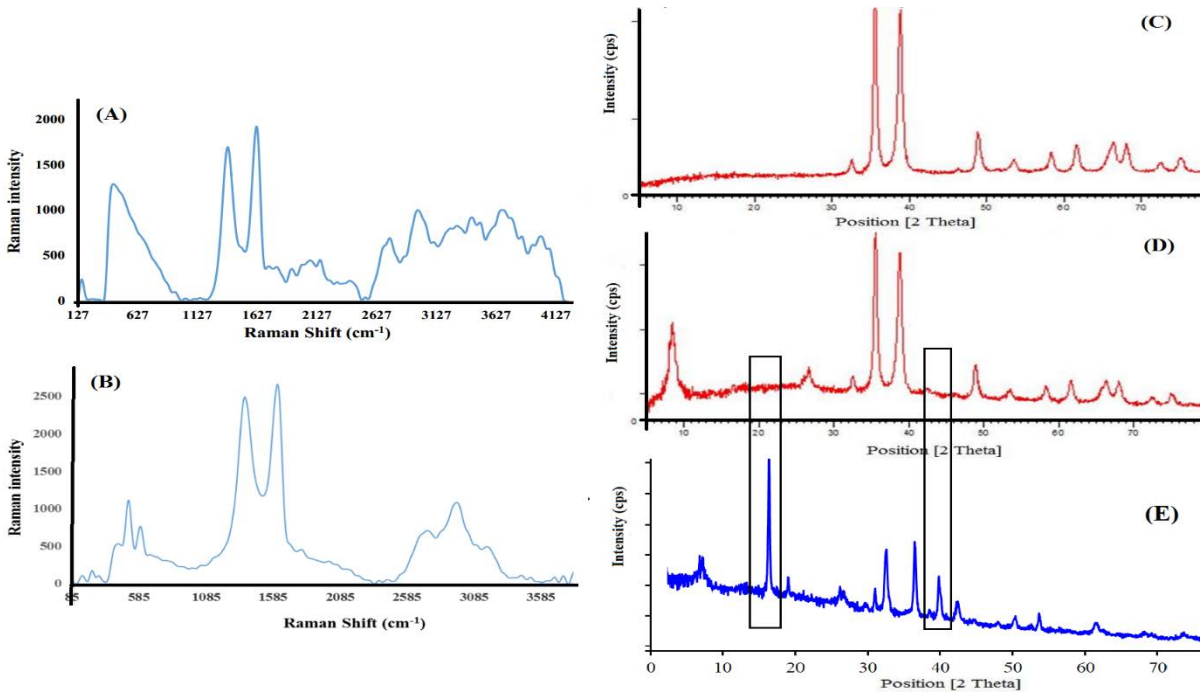

Fig. 1. Raman spectroscopy of (A) CuO and (B) GO–CuO. XRD patterns of (C) CuO nanoparticles and GO–CuO nanocomposite (D) before and (E) after desalination.

value of 0.96. The Scherrer equation suggested the average diameter of 20.7 nm for CuO nanoparticles.

3.3. Scanning electron microscopy

In a typical nanomaterial, an understanding of its microscopic structure is necessary to evaluate the features of the material. The morphology of the as-prepared GO and GO–CuO nanocomposite was investigated using FESEM. As can be seen in the FESEM image (Fig. 2(A)) the GO nanostructured films (sheets) are clearly formed. Fig. 2(B) indicates the presence of CuO nanoparticles which spread well onto the surface of GO sheets. In order to verify the presence of the desired elements, an EDX elemental analysis was performed on the GO–CuO nanocomposite (Fig. 2(C)). The results confirmed the presence of Cu (33.74% w/w), C (53.13% w/w) and O (13.13% w/w) elements on the GO–CuO. As evident from the obtained results the presence of carbon in the highest percentage is due to the fact that GO is the substrate for copper oxide. Additionally, EDX mapping (Fig. 2(C)) was applied for GO–CuO nanocomposite after desalination. As can be seen, the expected elements (carbon, oxygen, copper, sodium, potassium and chlorine) are well dispersed on the nanocomposite surface with appropriate weight percentage as 40.7%, 30.7%, 13.4%, 5.8%, 1.3% and 5.4% for C, O, Cu, Na, K and Cl, respectively.

3.4. Transmission electron microscopy

Fig. 3(A) shows the TEM micrograph of CuO nanoparticles. The TEM micrograph depicted the nano-size CuO with an average 20 nm size of nanoparticles. Fig. 3(B) illustrates that the graphene nanosheets are present in the form of stacked layers. Fig. 3(C) corresponds to the GO sheets after establishing with CuO nanoparticles (magnification ×12,000). It is clear that the CuO nanoparticles are well dispersed on the surface of GO sheets. Besides, the TEM image with high resolution (Fig. 3(D)) also specified that the GO sheets have prevented CuO nanoparticles from aggregation and vice versa.

3.5. Specific surface area analysis

To obtain the adsorbents specific surface area, pore volume and pore size, BET–BJH analysis were performed for GO and GO–CuO nanocomposite. Figs. 4(A) and (B) show GOs adsorption–desorption isotherm and BET linear graph, respectively. BET graph gives valuable information about N_2 gas volume (cm^3/g), specific surface area (m^2/g) and total pore volume (cm^3/g) of the adsorbent. BJH profile can ascribe the pore size distribution (nm) in the range of 1–100 nm. Figs. 4(C) and (D) show the adsorption–desorption isotherm and BET profile of GO–CuO, respectively. Hence, the specific surface area obtained was 133.28 and 76.97 m^2/g for GO and GO–CuO, respectively. Pore diameter was calculated to be 7.0 nm for GO and 9.2 nm for GO–CuO nanocomposite. These indicate that the specific surface area of GO doped with CuO nanoparticles (GO–CuO) was decreased to 42%, while the diameter of the pores is increased to 15.5% as compared with unmodified GO. Additionally, BET–BJH techniques are also used for analysing GO–CuO nanocomposite after desalination (Figs. 4(E) and (F)). After desalinate, the BET surface area declined to 16.6 m^2/g, indicating that the active adsorption sites were probably occupied with Na^+ and K^+ ions.

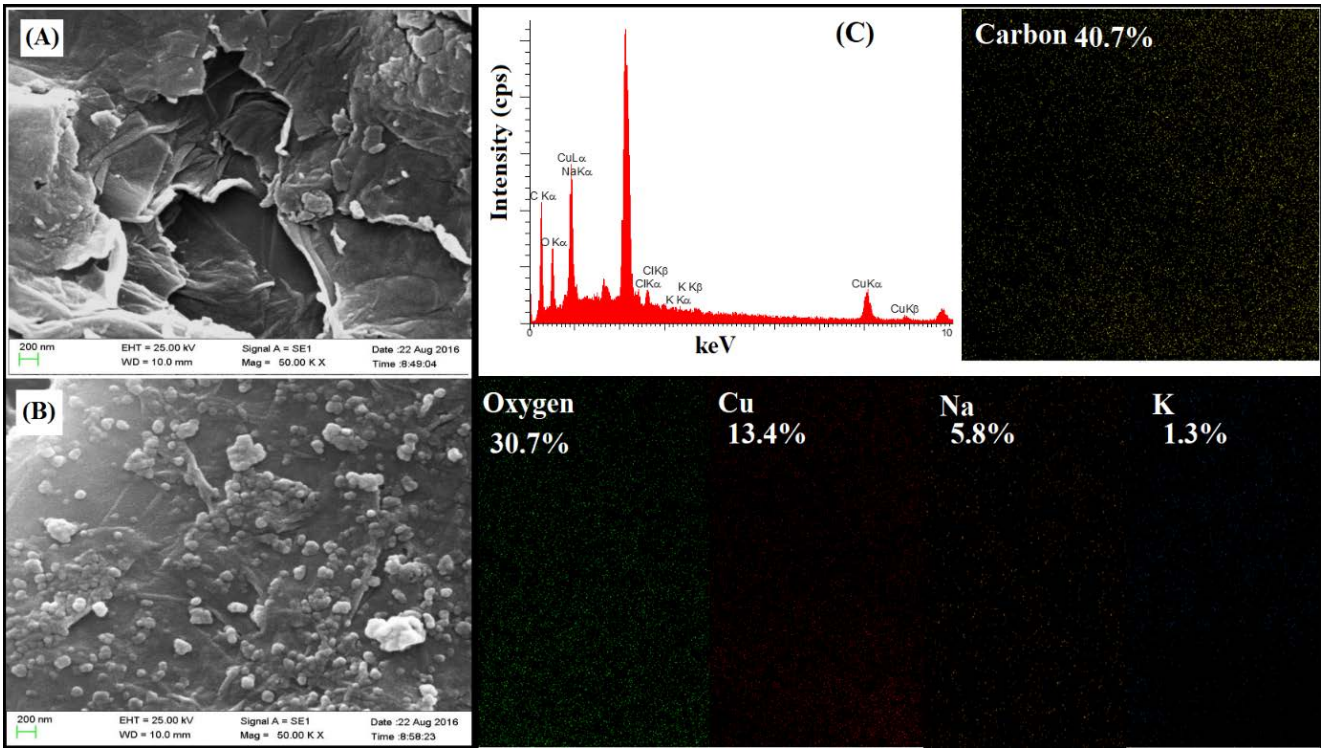

Fig. 2. FESEM micrograph of (A) graphene oxide and (B) GO–CuO nanocomposite. (C) EDX spectrum of GO–CuO nanoparticles after desalination and elements mapping analysis of carbon, oxygen, copper (Cu), sodium (Na) and potassium (K).

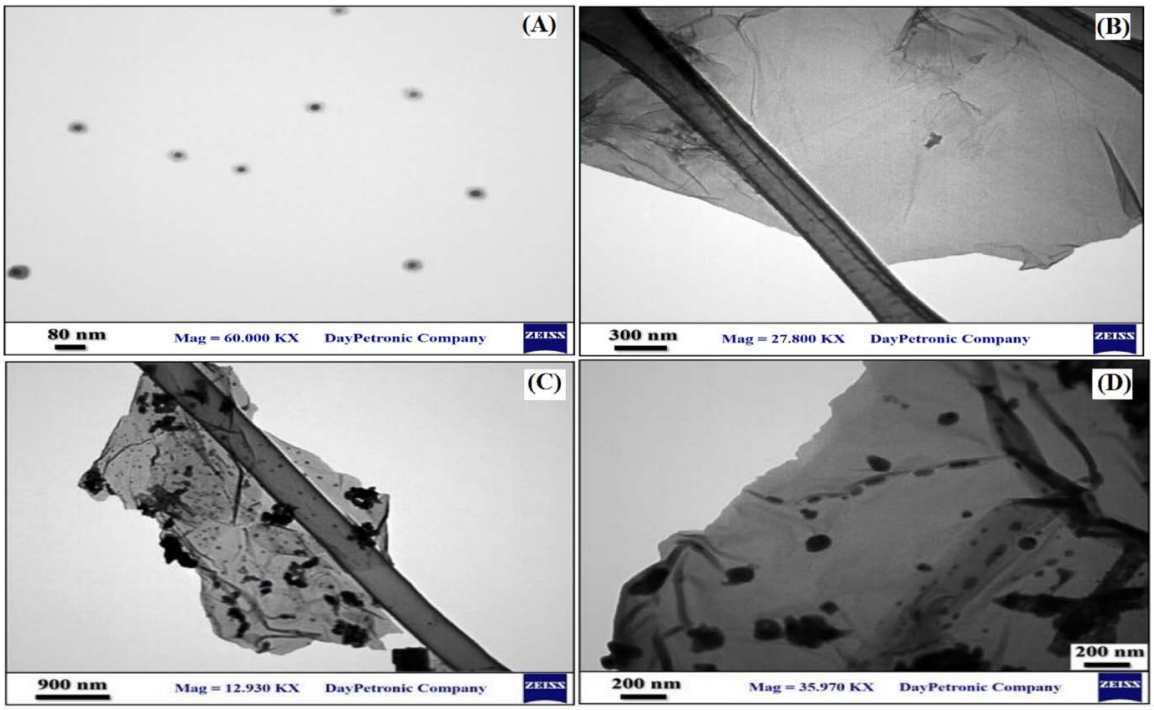

Fig. 3. TEM micrographs of (A) CuO nanoparticles, (B) graphene oxide, and GO–CuO nanocomposite with magnification of (C) ×12,000 and (D) ×35,000.

3.6. Parametric studies

3.6.1. pH study

The solution's pH is an important parameter in desalination process since it can control the ions sorption on the solid's surfaces, dissociation of functional groups, and the adsorbent/adsorbate degree of ionization. Zeta potential was studied for GO–CuO at different pH (Fig. 5(A)) which provided that the pH of point zero charge (pH_{PZC}) is 5.83. Given that the adsorbent possesses isoelectric charge at pH 5.83. Besides, at pH less than 5.83, adsorbent possess positive surface charge and at pH greater than 5.83 its change changes to negative charges (Fig. 5(B)). Therefore, at pH > pH_{PZC} the desalination and removal efficiency of sodium and potassium ions are the highest values. Since, the adsorption sites on the adsorbent increase by deprotonating of carboxyl groups that adsorb the positively charged sodium and potassium ions. However, the effect of pH on desalination performance was investigated by varying the pH from 5 to 8 when 0.1 g of GO–CuO adsorbent was used (Figs. 5(C) and (D)). The pH investigations indicated that by increasing the pH, the desalination efficiency increases as well. Hence, pH = 7.2 is selected as the optimum condition for further analysis. This is because the pH of Gulf of Oman seawater is equal to 7.2 and also that the removal efficiency does not increase significantly from pH 7.2 to pH 8.

3.6.2. Adsorption time

The effect of contact time on the adsorption of Na^+ and K^+ on GO–CuO was investigated for Gulf of Oman seawater (50 mL of Na^+ = 1,870 mg/L and K^+ = 920 mg/L solution and 100 mg of adsorbent). Fig. 6(A) shows that the adsorption efficiency for Na^+ and K^+ ions increases with an increase in the contact time from 5 to 20 min. The adsorption efficiency remains almost constant up to 60 min since sorption process reaches its equilibrium. Thus, 30 min is selected as an optimum time for desalination.

3.7. Adsorption capacity and isotherm

The adsorption capacity of the adsorbent (Q_e) was carried out by varying the concentration of Na^+ and K^+ ions of Gulf of Oman seawater as shown in Fig. 6(B). In particular, upon increasing the ions concentration the Q_e values for Na^+ and K^+ increases until all the adsorption sites are occupied (reaching equilibrium). In order to validate the experimental process and adsorption mechanism, the adsorption isotherm models were considered thoroughly [32,33]. Isotherm models can also explain the possible interactions between the adsorbent materials and adsorbed analytes. Hence, Langmuir, Freundlich and Temkin isotherms models were examined [34]. Langmuir isotherm describes the monolayer sorption onto the homogeneous surface with a single layer, where there is no interaction between the adsorbed molecules and the active sites of adsorbent [35,36]. Additionally, the sorption energy is constant and the adsorbent has a limited capacity for adsorbed [35,36]. Eq. (5) expresses the Langmuir isotherm:

$$Q_e = \frac{Q_m K_L C_e}{1 + K_L C_e} \tag{5}$$

where C_e is the residual concentration (mg/L), Q_e is the equilibrium sorption capacity (mg/g), K_L is the Langmuir constant

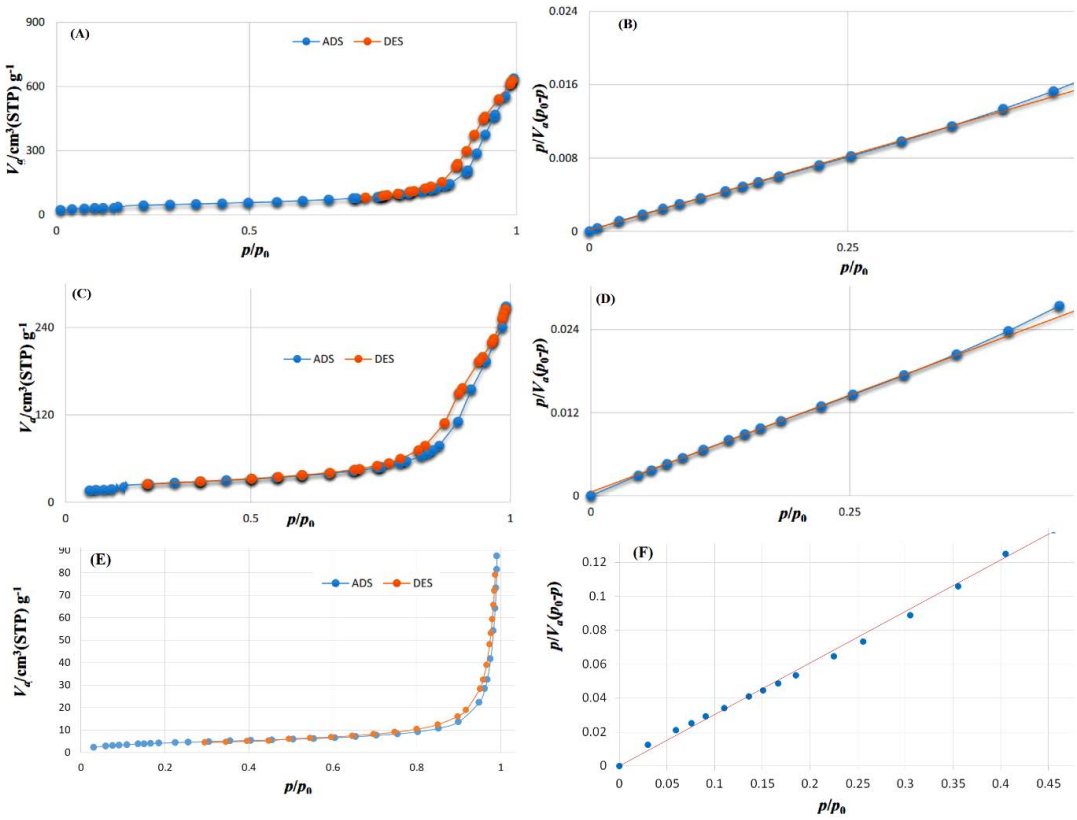

Fig. 4. (A) Adsorption–desorption isotherm and (B) BET profile of GO. (C) Adsorption–desorption isotherm and (D) BET profile of GO–CuO. (E) Adsorption–desorption isotherm and (F) BET profile for after desalination process.

related to heat adsorption (L/mg) and Q_m is the maximum adsorption capacity (mg/g) [3,23]. The Q_m value can be obtained from a linearized form of Langmuir (Fig. 7(A)) by plotting $1/Q_e$ vs. $1/C_e$. Hence, the values of Langmuir parameters for Na^+ and K^+ ions are listed in Table 1.

Freundlich isotherm describes the multilayer interactions between molecules adsorbed onto the heterogeneous surface [37,38]. Linearized form of Freundlich isotherm is plotted (Fig. 7(B)) based on Eq. (6):

$$Q_e = K_F C_e^{1/n} \tag{6}$$

where K_F is the Freundlich constant [(mg/g)/(mg/g)$^{1/n}$] and n reflects the degree of nonlinearity and surface heterogeneity. The highest heterogeneity occurs when the n value is close to zero. If the value of n is between 0 and 1, the adsorption is nonlinear. When n equals to 1, the adsorption is linear. The n values less than 1 ascribe the chemisorption and those greater than 1 describes physisorption process [39]. The values for Freundlich parameters are given in Table 1.

Temkin isotherm similar to the Freundlich model describes the heterogeneous surface by considering the indirect interactions between the adsorbed molecules. Moreover, it determines heat adsorption process [40]. The linearized form of Temkin can be represented using Eq. (7) as follows [34]:

$$Q_e = B \ln(A_T C_e) \tag{7}$$

$$B = \frac{RT}{\beta} \tag{8}$$

where A_T is the Temkin constant (L/g), B is the constant related to β (5.1), β is the heat of sorption (kJ/mol), R is the universal gas constant (0.008314 kJ/mol) and T is the temperature (K). Fig. 7(C) represents the linearized graph of Temkin model and the parameters values are listed in Table 1.

Table 1 represents that the Langmuir isotherm is applicable to validate the experimental data due to the high value of R^2 (coefficient of determination) as compared with Freundlich and Temkin models. The values of n and B indicated that the adsorption process follows a physical adsorption. Since $n > 1$ and $B < 20$ kJ/mol, the adsorption is a physisorption mechanism [41]. Thus, adsorption of Na^+ and K^+ ions from seawater using GO–CuO followed a monolayer pattern with physical adsorption mechanism.

3.8. Kinetic study

The sorption rate of Na^+ and K^+ ions from Gulf of Oman seawater was explained with pseudo-first-order, pseudo-second-order and intraparticle diffusion models. Besides, adsorption kinetics depends on the physical and chemical properties of the adsorbent material. This can also affect the adsorption mechanism. Additionally, kinetic models can be used in order to describe the adsorption

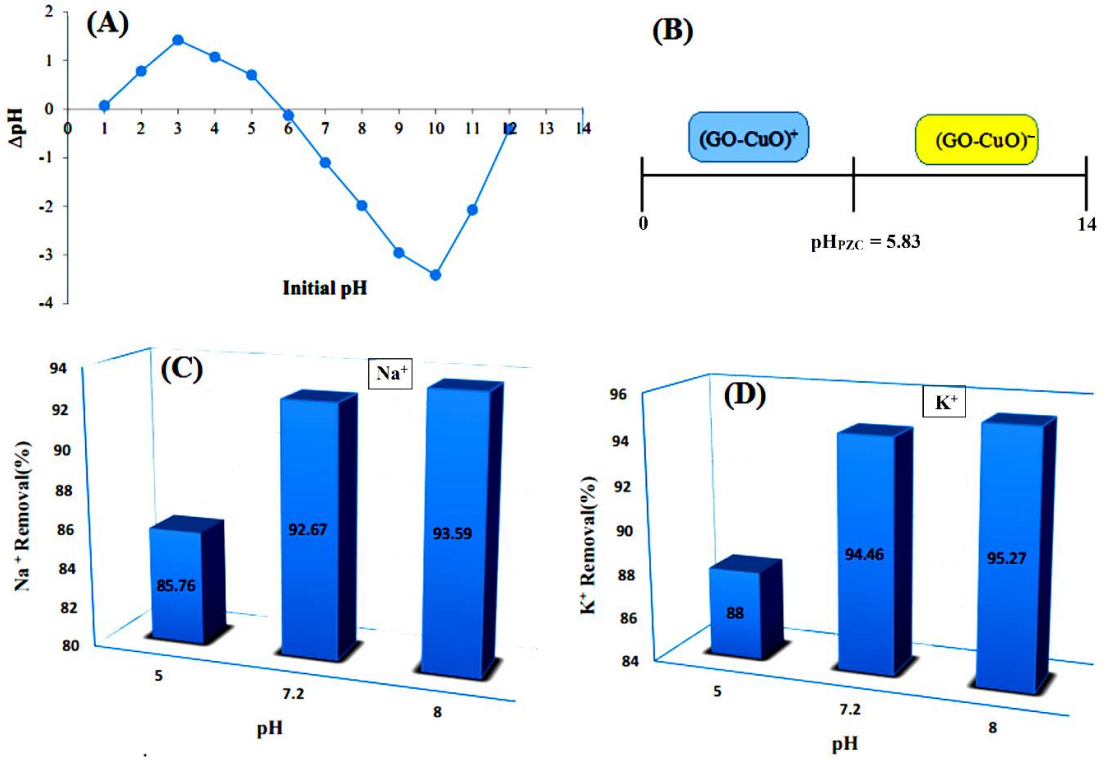

Fig. 5. (A) pH_{PZC} and (B) surface charge of adsorbent. Effect of pH on (C) sodium and (D) potassium adsorption from Gulf of Oman seawater.

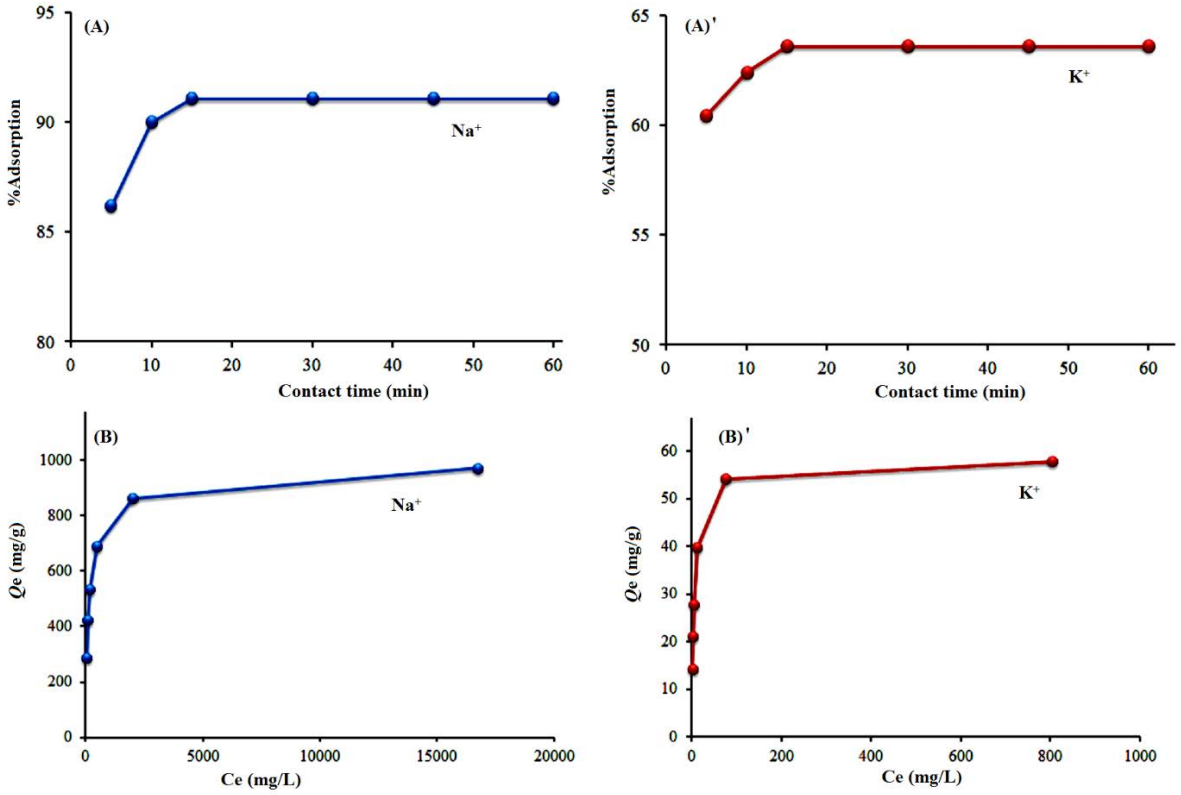

Fig. 6. (A) Effect of contact time on the adsorption of Na^+ and K^+ from Gulf of Oman seawater using GO–CuO. (B) Adsorption isotherm on adsorption capacity.

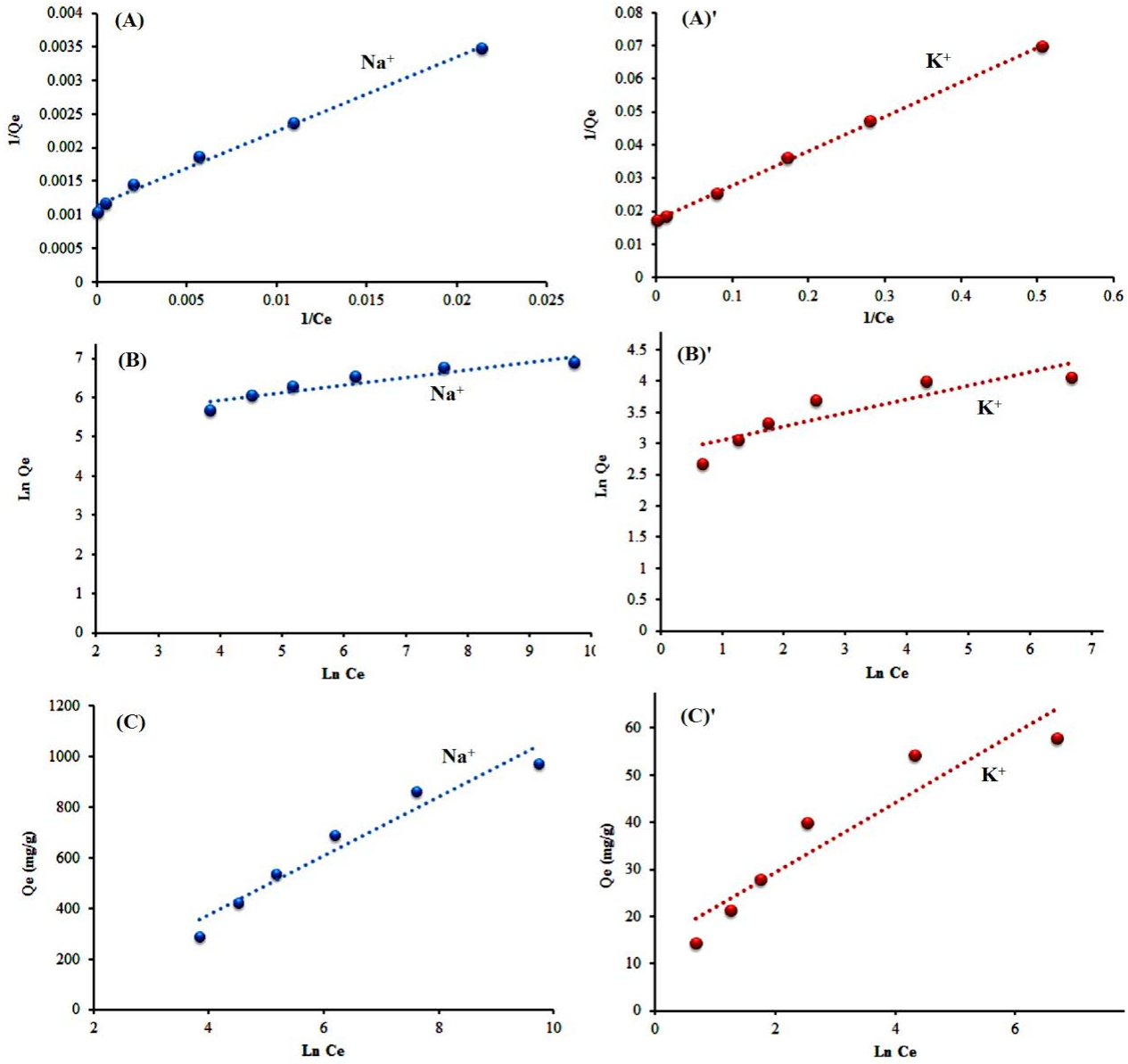

Fig. 7. (A) Langmuir, (B) Freundlich and (C) Temkin isotherms for sorption of Na^+ and K^+ from Gulf of Oman seawater samples.

Table 1
Langmuir, Freundlich and Temkin models parameters for sorption of Na^+ and K^+ from Gulf of Oman seawater using GO–CuO

Isotherm	Parameters	Na^+	K^+
Langmuir	Q_m (mg/g)	909	57
	K_L (L/mg)	0.009	0.165
	R^2	0.992	0.999
Freundlich	K_F [(mg/g)/(mg/g)$^{1/n}$]	123	14
	n	5.1	4.6
	R^2	0.859	0.797
Temkin	A_T (L/g)	2.07	6.17
	B (kJ/mol)	0.116	0.007
	R^2	0.946	0.889

mechanism, control the mass transfer and process of chemical reactions.

Pseudo-first-order is simple and widely used as a kinetic model for studying the uptake rate between sorbent and liquid phase [42]. This model is expressed by Eq. (9):

$$Q_t = Q_e(1 - e^{-k_1 t}) \tag{9}$$

where Q_e is the experimental sorption capacity (mg/g), Q_t is the sorption capacity at a time t, k_1 is the first-order rate constant (min^{-1}). The values of parameters are obtained from the linear graph (Figs. 8(A) and (B)), and the obtained values are listed in Table 2.

Pseudo-second-order kinetic indicates that the adsorption capacity of the adsorbent is proportional to its occupied

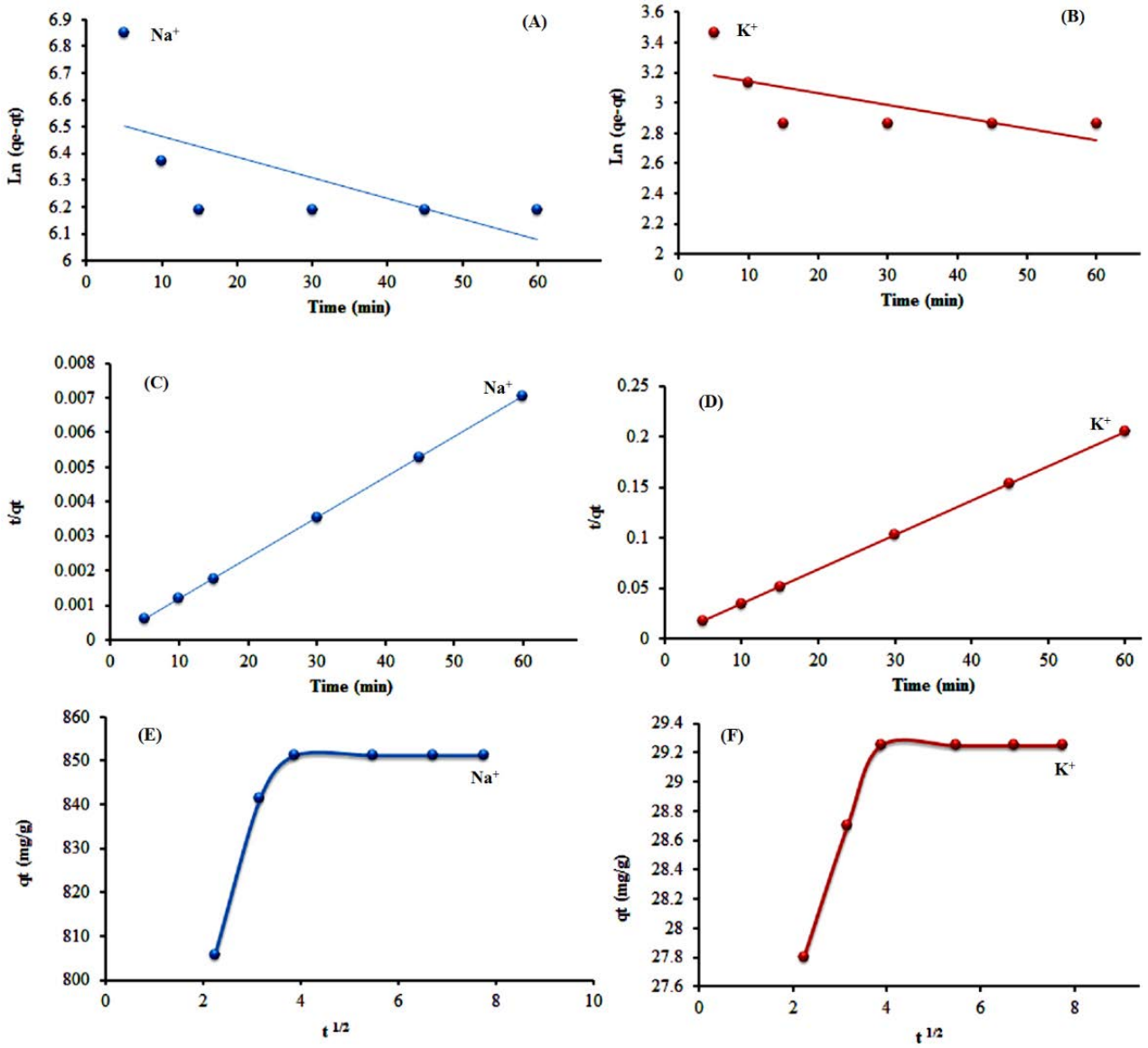

Fig. 8. Linearized graphs of kinetic models (A) and (B) pseudo-first-order for Na^+ and K^+, (C) and (D) pseudo-second-order for Na^+ and K^+ and (E) and (F) intraparticle diffusion for uptake of Na^+ and K^+ ions from Gulf of Oman seawater using GO–CuO.

active sites [42]. Moreover, this model describes the formation of bonds from sharing or exchanging electrons between the adsorbent and the adsorbed [43]. Pseudo-second-order model is represented by Eq. (10) [44]:

$$Q_t = \frac{Q_e k_2 t}{1 + k_2 Q_e t} \tag{10}$$

where Q_e (mg/g) is the experimental sorption capacity and k_2 is the second-order constant (g/mg min). The parameters values are calculated from the slope and intercept of the linear graph shown in Figs. 8(C) and (D), and the obtained values are given in Table 2.

Weber and Morris kinetics is known as intraparticle diffusion model and can be expressed by Eq. (11) as follow:

$$Q_t = k_{id} t^{1/2} + C_i \tag{11}$$

where the C_i is the boundary layer, k_{id} is Weber and Morris constant. If the value for C_i is high, the effect of the boundary layer would be significant. The linearized graph was obtained by plotting q_t against $t^{1/2}$ (Figs. 8(E) and (F)). In the graph, if the line passes from zero, the adsorption rate is only controlled by an intraparticle diffusion mechanism. In the graph, the first sharp step is corresponding to fast sorption on the surface of adsorbent and the second step is related to the gradual adsorption process [45]. The parameters values are listed in Table 2.

Regarding Table 2, the pseudo-second-order is well fitted to the experimental data as compared with

Table 2
Kinetic parameters for sorption of Na^+ and K^+ from Gulf of Oman seawater using GO–CuO

Kinetic models	Parameters	Na^+	K^+
Pseudo-first-order	Q_e (mg/g)	704	26
	k_1 (min^{-1})	0.0077	0.0079
	R^2	0.398	0.494
Pseudo-second-order	Q_e (mg/g)	10,000	295
	k_2 (g/mg min)	0.0000001	0.00001
	R^2	0.979	0.999
Intraparticle diffusion	$k_{id,1}$	283	8.9
	C_1	7,450	258
	R_1^2	0.943	0.996
	$k_{id,2}$	8,513	292
	C_2	–	–
	R_2^2	N/A	N/A

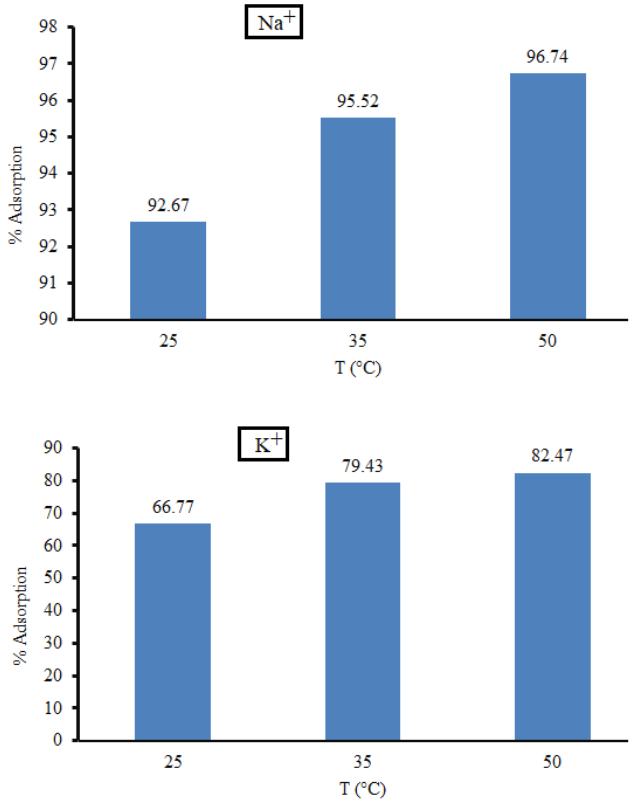

Fig. 9. Effect of temperature on the adsorption of sodium (Na^+) and potassium (K^+) from Gulf of Oman seawater samples.

pseudo-first-order due to the high value of R^2. Besides, pseudo-second-order suggested appropriate theoretical q_e values for Na^+ and K^+ uptake from Gulf of Oman seawater. Additionally, adsorption rate was controlled by intraparticle diffusion due to high values of C_1 and lower slope of the second step of the graph.

3.9. Temperature study

Fig. 9 shows the effect of temperature on the efficiency of Na^+ and K^+ removal from Gulf of Oman seawater at normal pH ~7.2 using 0.1 g of GO–CuO adsorbent. Different temperature values from 25°C to 50°C were selected due to the climatic conditions of South of Iran. By increasing the temperature from 25°C to 50°C, the removal efficiency of Na^+ and K^+ increased from 4.7% and 15.7%, respectively. This could be explained by the higher increase in the ionization rate of K^+ comparing with that of Na^+ when the temperature rises. Thus, more potassium ions would be absorbed by the sorbent at higher temperatures. Besides, increasing the temperature leads to hydration of Na^+ and K^+, therefore, the removal efficiency was improved for both ions as the temperature rises.

3.10. Regeneration

Effective regeneration of the newly prepared GO–CuO nanocomposite is essential to prove its affordable applicability as an adsorbent. The reusability of GO–CuO adsorbent was investigated by desorption of Na^+ and K^+ ions using 5 mL of HCl (0.1 M) after each removal process for 10 adsorption–desorption cycles. After each cycle, the GO–CuO was washed with excess distilled water and reused for the next experiment. For first cycle, adsorption efficiency obtained was 93% and 70% for Na^+ and K^+, respectively. After continuous adsorption process for five times the adsorption efficiency declines to 87% for Na^+ and 61% for K^+. Hence, based on the results, since the adsorption efficiency was not changed significantly after five continues removal procedures, the GO–CuO nanocomposite is reusable for at least five times.

4. Conclusion

In this study, a GO–CuO nanocomposite was synthesized, characterized and applied for desalination of sodium and potassium ions from Gulf of Oman seawater. TEM micrographs confirmed the morphology of synthesized graphene oxide as nanosheets and CuO as nanoparticles with an average diameter of 20 nm. BET–BJH techniques indicated high surface area of the nanocomposites with porous structure. The newly synthesized GO–CuO nanocomposite provided high removal efficiency of 96.74% and 82.47%, respectively, for sodium and potassium ions from Gulf of Oman seawater samples. Isotherm models were studied and the Langmuir was found to be the best isotherms to evaluate the experimental data. Kinetic studies suggested that the rate of ions adsorption onto GO–CuO follows a pseudo-first-order. Hence, isotherm and kinetic models suggested a monolayer adsorption pattern with physical adsorption mechanism for the removal of Na^+ and K^+ ions using GO–CuO. Moreover, the results show that the GO–CuO nanocomposite can be used as an effective sorbent in seawater desalination.

Acknowledgements

The authors would like to thank the Islamic Azad University (Tabriz branch) for facilitation and financial support through the Research Grants. Also, the authors sincerely thank Miss. Habibeh Eskandari (Ph.D. candidate) for her contribution in atomic emission spectrometry analysis.

References

[1] K. Park, S.Y. Hong, J.W. Lee, K.C. Kang, Y.C. Lee, M.-G. Ha, J.D. Lee, A new apparatus for seawater desalination by gas hydrate process and removal characteristics of dissolved minerals (Na^+, Mg^{2+}, Ca^{2+}, K^+, B^{3+}), Desalination, 274 (2011) 91–96.

[2] K.C. Kang, P. Linga, K. Park, S.-J. Choi, J.D. Lee, Seawater desalination by gas hydrate process and removal characteristics of dissolved ions (Na^+, K^+, Mg^{2+}, Ca^{2+}, B^{3+}, Cl^-, SO_4^{2-}), Desalination, 353 (2014) 84–90.

[3] S. Burn, M. Hoang, D. Zarzo, F. Olewniak, E. Campos, B. Bolto, O. Barron, Desalination techniques – a review of the opportunities for desalination in agriculture, Desalination, 364 (2015) 2–16.

[4] B. Kwakye-Awuah, E. Von-Kiti, I. Nkrumah, R. Erdoo Ikyreve, I. Radecka, C. Williams, Parametric, equilibrium, and kinetic study of the removal of salt ions from Ghanaian seawater by adsorption onto zeolite X, Desal. Wat. Treat., 57 (2016) 21654–21663.

[5] Y. You, V. Sahajwalla, M. Yoshimura, R.K. Joshi, Graphene and graphene oxide for desalination, Nanoscale, 8 (2016) 117–119.

[6] H. Fakharian, H. Ganji, A. Naderifar, Desalination of high salinity produced water using natural gas hydrate, J. Taiwan Inst. Chem. Eng., 72 (2017) 157–162.

[7] S.G. Kim, D.H. Hyeon, J.H. Chun, B.-H. Chun, S.H. Kim, Nanocomposite poly (arylene ether sulfone) reverse osmosis membrane containing functional zeolite nanoparticles for seawater desalination, J. Membr. Sci., 443 (2013) 10–18.

[8] L. Zhou, Y. Tan, J. Wang, W. Xu, Y. Yuan, W. Cai, S. Zhu, J. Zhu, 3D self-assembly of aluminium nanoparticles for plasmon-enhanced solar desalination, Nat. Photonics, 10 (2016) 393–398.

[9] H. Dong, L. Zhao, L. Zhang, H. Chen, C. Gao, W.S.W. Ho, High-flux reverse osmosis membranes incorporated with NaY zeolite nanoparticles for brackish water desalination, J. Membr. Sci., 476 (2015) 373–383.

[10] M. Zargar, Y. Hartanto, B. Jin, S. Dai, Understanding functionalized silica nanoparticles incorporation in thin film composite membranes: interactions and desalination performance, J. Membr. Sci., 521 (2017) 53–64.

[11] M.J. Park, G.M. Nisola, A.B. Beltran, R.E.C. Torrejos, J.G. Seo, S.-P. Lee, H. Kim, W.-J. Chung, Recyclable composite nanofiber adsorbent for Li^+ recovery from seawater desalination retentate, Chem. Eng. J., 254 (2014) 73–81.

[12] H. Demey, T. Vincent, M. Ruiz, M. Nogueras, A.M. Sastre, E. Guibal, Boron recovery from seawater with a new low-cost adsorbent material, Chem. Eng. J., 254 (2014) 463–471.

[13] G. Zelmanov, R. Semiat, Boron removal from water and its recovery using iron (Fe^{+3}) oxide/hydroxide-based nanoparticles (NanoFe) and NanoFe-impregnated granular activated carbon as adsorbent, Desalination, 333 (2014) 107–117.

[14] L. Xu, J.-T. Hu, H.-J. Ma, C.-J. Ling, M.-H. Wang, R.-F. Shen, X.-J. Guo, Y.-N. Wang, J.-Y. Li, G.-Z. Wu, Amidoxime-based adsorbents prepared by cografting acrylic acid with acrylonitrile onto HDPE fiber for the recovery of uranium from seawater, Nucl. Sci. Technol., 28 (2017) 45–57.

[15] Q. Zhao, N. Chen, D. Zhao, X. Lu, Thermoresponsive magnetic nanoparticles for seawater desalination, ACS Appl. Mater. Interfaces, 5 (2013) 11453–11461.

[16] S. Shahabuddin, N.M. Sarih, S. Mohamad, S.N.A. Baharin, Synthesis and characterization of Co_3O_4 nanocube-doped polyaniline nanocomposites with enhanced methyl orange adsorption from aqueous solution, RSC Adv., 6 (2016) 43388–43400.

[17] S. Shahabuddin, N. Muhamad Sarih, S. Mohamad, J. Joon Ching, $SrTiO_3$ nanocube-doped polyaniline nanocomposites with enhanced photocatalytic degradation of methylene blue under visible light, Polymers, 8 (2016) 27–35.

[18] S. Shahabuddin, N.M. Sarih, M. Afzal Kamboh, H. Rashidi Nodeh, S. Mohamad, Synthesis of polyaniline-coated graphene oxide@$SrTiO_3$ nanocube nanocomposites for enhanced removal of carcinogenic dyes from aqueous solution, Polymers, 8 (2016) 305–314.

[19] B. Feng, K. Xu, A. Huang, Covalent synthesis of three-dimensional graphene oxide framework (GOF) membrane for seawater desalination, Desalination, 394 (2016) 123–130.

[20] X. Wang, G. Ou, N. Wang, H. Wu, Graphene-based recyclable photo-absorbers for high-efficiency seawater desalination, ACS Appl. Mater. Interfaces, 8 (2016) 9194–9199.

[21] K. Xu, B. Feng, C. Zhou, A. Huang, Synthesis of highly stable graphene oxide membranes on polydopamine functionalized supports for seawater desalination, Chem. Eng. Sci., 146 (2016) 159–165.

[22] W.A. Wan Ibrahim, H. Rashidi Nodeh, M.M. Sanagi, Graphene-based materials as solid phase extraction sorbent for trace metal ions, organic compounds, and biological sample preparation, Crit. Rev. Anal. Chem., 46 (2016) 267–283.

[23] X. Gu, Y. Yang, Y. Hu, M. Hu, C. Wang, Fabrication of graphene-based xerogels for removal of heavy metal ions and capacitive deionization, ACS Sustain. Chem. Eng., 3 (2015) 1056–1065.

[24] R. Mukherjee, P. Bhunia, S. De, Impact of graphene oxide on removal of heavy metals using mixed matrix membrane, Chem. Eng. J., 292 (2016) 284–297.

[25] A. Aghigh, V. Alizadeh, H.Y. Wong, M.S. Islam, N. Amin, M. Zaman, Recent advances in utilization of graphene for filtration and desalination of water: a review, Desalination, 365 (2015) 389–397.

[26] H.M. Hegab, L. Zou, Graphene oxide-assisted membranes: fabrication and potential applications in desalination and water purification, J. Membr. Sci., 484 (2015) 95–106.

[27] H.R. Naika, K. Lingaraju, K. Manjunath, D. Kumar, G. Nagaraju, D. Suresh, H. Nagabhushana, Green synthesis of CuO nanoparticles using *Gloriosa superba* L. extract and their antibacterial activity, J. Taibah Univ. Sci., 9 (2015) 7–12.

[28] M. Nasrollahzadeh, S.M. Sajadi, A. Rostami-Vartooni, S.M. Hussin, Green synthesis of CuO nanoparticles using aqueous extract of *Thymus vulgaris* L. leaves and their catalytic performance for N-arylation of indoles and amines, J. Colloid Interface Sci., 466 (2016) 113–119.

[29] T. Pandiyarajan, R. Udayabhaskar, S. Vignesh, R.A. James, B. Karthikeyan, Synthesis and concentration dependent antibacterial activities of CuO nanoflakes, Mater. Sci. Eng., C, 33 (2013) 2020–2024.

[30] B. Ramazanzadeh, A. Jahanbin, M. Yaghoubi, N. Shahtahmassbi, K. Ghazvini, M. Shakeri, H. Shafaee, Comparison of antibacterial effects of ZnO and CuO nanoparticles coated brackets against *Streptococcus mutans*, J. Dent., 16 (2015) 200–207.

[31] M. Ahamed, H.A. Alhadlaq, M.A. Khan, P. Karuppiah, N.A. Al-Dhabi, Synthesis, characterization, and antimicrobial activity of copper oxide nanoparticles, J. Nanomater., 1 (2014) 17–28.

[32] S. Abbaszadeh, S.R. Wan Alwi, N. Ghasemi, H. Rashidi Nodeh, C. Colin Webb, I.I. Muhamad, Use of pristine papaya peel to remove Pb(II) from aqueous solution, Chem. Eng. Trans., 45 (2015) 961–966.

[33] C. Srilakshmi, R. Saraf, Ag-doped hydroxyapatite as efficient adsorbent for removal of Congo red dye from aqueous solution: synthesis, kinetic and equilibrium adsorption isotherm analysis, Microporous Mesoporous Mater., 219 (2016) 134–144.

[34] M. Rahimi, M. Vadi, S. Branch, I. Sarvestan, Langmuir, Freundlich and Temkin adsorption isotherms of propranolol on multi-wall carbon nanotubes, J. Mod. Drug Discovery Drug Delivery Res., 2 (2014) 18–20.

[35] Y.S. Ho, J.F. Porter, G. McKay, Equilibrium isotherm studies for the sorption of divalent metal ions onto peat: copper, nickel and lead single component systems, Water, Air, Soil Pollut., 141 (2002) 1–33.

[36] M.A. Kamboh, W.A. Wan Ibrahim, H. Rashidi Nodeh, M.M. Sanagi, S.T.H. Sherazi, The removal of organophosphorus pesticides from water using a new amino-substituted calixarene-based magnetic sporopollenin, New J. Chem., 40 (2016) 3130–3138.

[37] H. Rashidi Nodeh, W.A. Wan Ibrahim, I. Ali, M.M. Sanagi, Development of magnetic graphene oxide adsorbent for the removal and preconcentration of As (III) and As (V) species from environmental water samples, Environ. Sci. Pollut. Res., 23 (2016) 9759–9773.

[38] H. Rashidi Nodeh, H. Sereshti, Synthesis of magnetic graphene oxide doped with strontium titanium trioxide nanoparticles as a nanocomposite for the removal of antibiotics from aqueous media, RSC Adv., 6 (2016) 89953–89965.
[39] F. Gimbert, N. Morin-Crini, F. Renault, P.-M. Badot, G. Crini, Adsorption isotherm models for dye removal by cationized starch-based material in a single component system: error analysis, J. Hazard. Mater., 157 (2008) 34–46.
[40] I.H. Ali, H.A. Alrafai, Kinetic, isotherm and thermodynamic studies on biosorption of chromium (VI) by using activated carbon from leaves of *Ficus nitida*, Chem. Cent. J., 10 (2016) 36–47.
[41] A.O. Dada, A.P. Olalekan, A.M. Olatunya, O. Dada, Langmuir, Freundlich, Temkin and Dubinin–Radushkevich isotherms studies of equilibrium sorption of Zn^{2+} unto phosphoric acid modified rice husk, J. Appl. Chem., 3 (2012) 38–45.
[42] H. Daraei, A. Mittal, M. Noorisepehr, J. Mittal, Separation of chromium from water samples using eggshell powder as a low-cost sorbent: kinetic and thermodynamic studies, Desal. Wat. Treat., 53 (2015) 214–220.
[43] B. Subramanyam, A. Das, Study of the adsorption of phenol by two soils based on kinetic and isotherm modeling analyses, Desalination, 249 (2009) 914–921.
[44] M. Al-Shannag, Z. Al-Qodah, K. Bani-Melhem, M.R. Qtaishat, M. Alkasrawi, Heavy metal ions removal from metal plating wastewater using electrocoagulation: kinetic study and process performance, Chem. Eng. J., 260 (2015) 749–756.
[45] B.H. Hameed, I.A.W. Tan, A.L. Ahmad, Adsorption isotherm, kinetic modeling and mechanism of 2,4,6-trichlorophenol on coconut husk-based activated carbon, Chem. Eng. J., 144 (2008) 235–244.